J. Fluid Mech. (1998), *vol.* 374, *pp.* 285–303. Printed in the United Kingdom

On steady compressible flows with compact vorticity; the compressible Hill's spherical vortex

By D. W. MOORE[1] AND D. I. PULLIN[2]

[1]Department of Mathematics, Imperial College of Science, Technology and Medicine, Queens Gate, London SW7 2BZ, UK

[2]Graduate Aeronautical Laboratories 105-50, California Institute of Technology, Pasadena, CA 91125, USA

(Received 5 December 1997 and in revised form 18 June 1998)

We consider steady compressible Euler flow corresponding to the compressible analogue of the well-known incompressible Hill's spherical vortex (HSV). We first derive appropriate compressible Euler equations for steady homentropic flow and show how these may be used to define a continuation of the HSV to finite Mach number $M_\infty = U_\infty/C_\infty$, where U_∞, C_∞ are the fluid velocity and speed of sound at infinity respectively. This is referred to as the compressible Hill's spherical vortex (CHSV). It corresponds to axisymmetric compressible Euler flow in which, within a vortical bubble, the azimuthal vorticity divided by the product of the density and the distance to the axis remains constant along streamlines, with irrotational flow outside the bubble. The equations are first solved numerically using a fourth-order finite-difference method, and then using a Rayleigh–Janzen expansion in powers of M_∞^2 to order M_∞^4. When $M_\infty > 0$, the vortical bubble is no longer spherical and its detailed shape must be determined by matching conditions consisting of continuity of the fluid velocity at the bubble boundary. For subsonic compressible flow the bubble boundary takes an approximately prolate spheroidal shape with major axis aligned along the flow direction. There is good agreement between the perturbation solution and Richardson extrapolation of the finite difference solutions for the bubble boundary shape up to M_∞ equal to 0.5. The numerical solutions indicate that the flow first becomes locally sonic near or at the bubble centre when $M_\infty \approx 0.598$ and a singularity appears to form at the sonic point. We were unable to find shock-free steady CHSVs containing regions of locally supersonic flow and their existence for the present continuation of the HSV remains an open question.

1. Introduction

An understanding of the dynamics of compressible vortices is expected to be important for investigation of both shock–vortex and shock–turbulence interactions. Compressibility effects in vortex cores have been studied theoretically in a variety of geometries (Mack 1960; Brown 1965; Colonius, Lele & Moin 1991). Experiments on compressible starting vortices (Lee & Bershader 1994) show structure similar to that of wing-tip vortices. Theoretical studies of vortex structures capable of steady self-propagation though a compressible fluid have to date been limited to vortex pairs in which the compact vorticity was modelled by closed free streamlines (Moore & Pullin 1987; Heister *et al.* 1990). The hodograph method of Moore & Pullin (1987) can be extended to the study of vortex arrays modelling a free shear layer (Ardalan, Meiron

& Pullin 1995) but is restricted to structures containing stagnant vortex cores. These vortex states, although useful as a guide to the principal effects of compressibility, are not suitable for use in numerical shock–vortex interaction studies, where a compact vorticity and a smooth velocity field are needed to generate realistic initial states.

The objective of the present study is to present both numerical and analytical solutions to the compressible Euler equations representing the steady self-propagation of a vortex state which corresponds to a compressible analogue of the incompressible Hill's spherical vortex (HSV) (Hill 1894). This is chosen owing to its confined vorticity and simple analytical form when $M_\infty = 0$. In §2 we derive the basic equations governing the continuation of the HSV to the compressible domain, under the assumption of homentropic flow. Section 3 describes a fourth-order-accurate finite difference scheme for solving the homentropic compressible HSV (CHSV) equations. A perturbation method based on a Rayleigh–Janzen expansion is described in §3 and results from both the numerical and analytical methods are given in §4. We point out that the continuation to finite Mach number is not unique, and in the Appendix we discuss alternative continuations based on isenthalpic flow, although no analysis or numerical solutions are given for these vortex states. We note that numerical studies of the interaction of a shock with a preliminary second-order-accurate version of the present model of a compressible Hill's spherical vortex has already been reported (Samtaney & Pullin 1997). A similar study of the interaction of a shock with a weakly compressible Hill's spherical vortex has been given by Lixian, Sato & Shimizu (1997). These authors appear to use a model vortex consisting of the incompressible velocity field and a density field obtained from the leading-order Rayleigh–Janzen expansion.

2. Derivation of the governing equations

We start with the Euler equations for steady, inviscid and non-heat-conducting flow

$$\nabla H_0 = \boldsymbol{u} \wedge \boldsymbol{\omega} + T\,\nabla S, \tag{2.1}$$

$$\nabla \cdot (\rho \boldsymbol{u}) = 0, \tag{2.2}$$

and

$$(\boldsymbol{u} \cdot \nabla)\, S = 0, \tag{2.3}$$

with the immediate deduction that

$$(\boldsymbol{u} \cdot \nabla)\, H_0 = 0. \tag{2.4}$$

Here $\boldsymbol{u}(\boldsymbol{x})$ is the velocity, $p(\boldsymbol{x})$ the pressure, $\rho(\boldsymbol{x})$ the density, $S(\boldsymbol{x})$ the entropy, $T(\boldsymbol{x})$ the absolute temperature, $H_0(\boldsymbol{x}) = H(\boldsymbol{x}) + \frac{1}{2}\boldsymbol{u}^2$ the total enthalpy and $H(\boldsymbol{x})$ the enthalpy.

We now consider the formulation of a set of equations representing a compressible version of Hill's vortex. We employ spherical coordinates (r, θ), where where r is distance from the origin and θ is the polar angle measured from the downstream axis of symmetry. We use dimensionless coordinates, without change of notation, by setting to unity a, the radius of the incompressible Hill's spherical vortex, U_∞, the fluid speed at infinity and ρ_∞, the gas density at infinity. The velocity components u and v are defined by

$$\boldsymbol{u}(\boldsymbol{x}) = u_r(r, \theta)\, \boldsymbol{e}_r + u_\theta(r, \theta)\, \boldsymbol{e}_\theta, \tag{2.5}$$

where $\boldsymbol{e}_r, \boldsymbol{e}_\theta$ are unit vectors in the r- and θ-directions respectively. We can satisfy

continuity by the introduction of a stream function $\psi(r,\theta)$ defined by

$$u_r = \frac{1}{\rho\, r^2 \sin\theta}\,\frac{\partial\psi}{\partial\theta}, \tag{2.6}$$

and

$$u_\theta = -\frac{1}{\rho\, r \sin\theta}\,\frac{\partial\psi}{\partial r}, \tag{2.7}$$

and we note that $\psi(r,\theta)$ is made dimensionless against the product $a^2\rho_\infty U_\infty$. We shall express the governing equations in terms of $\rho(r,\theta)$ and $\psi(r,\theta)$. We note here that (2.3)–(2.4) imply that

$$S = S(\psi), \tag{2.8}$$

$$H_0 = H_0(\psi). \tag{2.9}$$

The vorticity of the motion is given by

$$\omega = \boldsymbol{e}_\phi \eta(r,\theta), \tag{2.10}$$

where $\boldsymbol{e}_\phi$ is orthogonal to $\boldsymbol{e}_r, \boldsymbol{e}_\theta$ and

$$\eta(r,\theta) = \frac{1}{r}\left(\frac{\partial(r\,u_\theta)}{\partial r} - \frac{\partial u_r}{\partial\theta}\right), \tag{2.11}$$

and Euler's equation (2.1) is, in component form,

$$\frac{\partial H_0}{\partial r} = \eta\, u_\theta + T\frac{\partial S}{\partial r}, \tag{2.12}$$

$$\frac{1}{r}\,\frac{\partial H_0}{\partial\theta} = -\eta\, u_r + \frac{T}{r}\,\frac{\partial S}{\partial\theta}. \tag{2.13}$$

Using (2.5)–(2.7) these can be expressed as

$$\frac{\eta}{\rho\, r\sin\theta}\,\frac{\partial\psi}{\partial r} = T\,\frac{\partial S}{\partial r} - \frac{\partial H_0}{\partial r}, \tag{2.14}$$

$$\frac{\eta}{\rho\, r\sin\theta}\,\frac{\partial\psi}{\partial\theta} = T\,\frac{\partial S}{\partial\theta} - \frac{\partial H_0}{\partial\theta}. \tag{2.15}$$

From (2.8)–(2.9) and (2.14)–(2.15) it then follows that

$$\frac{\eta}{\rho\, r\sin\theta} = T\frac{\mathrm{d}S}{\mathrm{d}\psi} - \frac{\mathrm{d}H_0}{\mathrm{d}\psi}. \tag{2.16}$$

This relationship was obtained by Vazsonyi (1945) for two-dimensional flows.

We define two cases of interest: homentropic flow, $S(\psi)$ = constant throughout the flow with $H_0 = H_0(\psi)$, and homenthalpic flow, $H_0(\psi)$ = constant throughout with $S = S(\psi)$. This latter case is discussed further in the Appendix. Here we consider only the homentropic case for which (2.16) becomes

$$\frac{\eta}{\rho\, r\sin\theta} = -\frac{\mathrm{d}H_0}{\mathrm{d}\psi} \equiv V(\psi), \tag{2.17}$$

where the function $V(\psi)$, made dimensionless against $U_\infty/(\rho_\infty a^2)$, is at our disposal. Integrating (2.17) gives

$$H_0(\psi) = -\int_0^\psi V(\psi')\mathrm{d}\psi' + H_{00}, \tag{2.18}$$

where H_{00} is a constant of integration.

If we express η in terms of ψ and substitute into (2.17), then we find that

$$\mathrm{D}^2\psi - \frac{1}{\rho} N(\psi, \rho) = -\rho^2 r^2 \sin^2\theta \, V(\psi), \tag{2.19}$$

where the operator D^2 is defined by

$$\mathrm{D}^2 = \frac{\partial^2}{\partial r^2} + \frac{\sin\theta}{r^2} \frac{\partial}{\partial\theta} \left(\frac{1}{\sin\theta} \frac{\partial}{\partial\theta} \right); \tag{2.20}$$

and

$$N(f, g) = \frac{\partial f}{\partial r} \frac{\partial g}{\partial r} + \frac{1}{r^2} \frac{\partial f}{\partial\theta} \frac{\partial g}{\partial\theta}; \tag{2.21}$$

(2.19) is the first of the pair of governing equations.

We have not, so far, introduced thermodynamic state equations. It is now assumed that the fluid is a calorically perfect ideal gas. For homentropic flow it then follows that $p = A\rho^\gamma$ where A is a constant and γ is the ratio of specific heats. Equation (2.9) together with $H_0 = H + \frac{1}{2}\boldsymbol{u}^2$ then gives

$$\tfrac{1}{2}\boldsymbol{u}^2 + \frac{\gamma A \rho^{\gamma-1}}{\gamma - 1} = H_0(\psi). \tag{2.22}$$

Using (2.6)–(2.7) and (2.18) and eliminating the constant A in favour of the Mach number

$$M_\infty = U_\infty / C_\infty,$$

where C_∞ is the sound speed at infinity, then gives

$$\tfrac{1}{2} M_\infty^2 N(\psi, \psi) + \frac{r^2 \sin^2\theta \, \rho^{\gamma+1}}{(\gamma - 1)} = M_\infty^2 \rho^2 r^2 \sin^2\theta \left(- \int_0^\psi V(\psi') \, \mathrm{d}\psi' + H_{00} \right). \tag{2.23}$$

In the incompressible limit, the Hill's spherical vortex is obtained by the choice $V(\psi) = -\Omega_0$ where

$$\left.\begin{aligned} \Omega_0 &= \tfrac{15}{2} \qquad \text{(inside the HSV)}, \\ \Omega_0 &= 0 \qquad\quad \text{(outside the HSV)}. \end{aligned}\right\} \tag{2.24}$$

We retain this value of $V(\psi)$ for the compressible case and it is this that defines the present homentropic continuation of the HSV to $M_\infty > 0$. With our choice of $V(\psi)$, (2.19) and (2.23) become respectively

$$\mathrm{D}^2\psi - \frac{1}{\rho} N(\psi, \rho) = \Omega_0 \rho^2 r^2 \sin^2\theta, \tag{2.25}$$

$$\tfrac{1}{2} M_\infty^2 N(\psi, \psi) + r^2 \sin^2\theta \, \frac{\rho^{\gamma+1}}{(\gamma - 1)} = M_\infty^2 \rho^2 r^2 \sin^2\theta \; (H_{00} + \Omega_0 \psi), \tag{2.26}$$

or, if $q(r, \theta)$ is the speed of the fluid

$$\tfrac{1}{2} M_\infty^2 q^2 + \frac{\rho^{(\gamma-1)}}{(\gamma - 1)} = M_\infty^2 \, (H_{00} + \Omega_0 \psi). \tag{2.27}$$

However we know from our choice of scales that $q = 1$ and $\rho = 1$ at infinity, so that

$$H_{00} = \frac{1}{2} + \frac{1}{(\gamma - 1) M_\infty^2}. \tag{2.28}$$

We insist that the fluid speed and density are continuous across the vortex boundary. But Ω_0 is discontinuous across this boundary. To secure continuity of ρ, then, we must have $\psi = 0$ on the vortex boundary.

We can now state the mathematical problem as follows: we seek a stream function $\psi(r, \theta)$ a density field $\rho(r, \theta)$ and a vortex-boundary shape $r = R(\theta)$ such that, for $0 \leqslant \theta \leqslant \pi$,

$$\psi \sim \tfrac{1}{2} r^2 \sin^2 \theta \quad \text{as } r \to \infty, \tag{2.29}$$

$$\rho \to 1 \quad \text{as } r \to \infty, \tag{2.30}$$

$$\psi(R(\theta), \theta) = 0, \tag{2.31}$$

$$\frac{\partial \psi}{\partial r}\Big|_{r=R(\theta)} \quad \text{is continuous across } r = R(\theta), \tag{2.32}$$

and

$$\psi = O(r^2) \quad \text{as } r \to 0. \tag{2.33}$$

From (2.26)–(2.28) and (2.21), the coupled fields $\psi(r, \theta)$ and $\rho(r, \theta)$ must satisfy

$$\frac{\partial^2 \psi}{\partial r^2} + \frac{1}{r^2}\left(\frac{\partial^2 \psi}{\partial \theta^2} - \cot\theta \frac{\partial \psi}{\partial \theta}\right) - \frac{1}{\rho}\left(\frac{\partial \psi}{\partial r}\frac{\partial \rho}{\partial r} + \frac{1}{r^2}\frac{\partial \psi}{\partial \theta}\frac{\partial \rho}{\partial \theta}\right) = \Omega_0 \rho^2 r^2 \sin^2 \theta, \tag{2.34}$$

and

$$\frac{M_\infty^2}{2r^2 \sin^2 \theta}\left[\left(\frac{\partial \psi}{\partial r}\right)^2 + \frac{1}{r^2}\left(\frac{\partial \psi}{\partial \theta}\right)^2\right] + \frac{\rho^2\left(\rho^{\gamma-1} - 1\right)}{\gamma - 1} = M_\infty^2 \left(\tfrac{1}{2} + \Omega_0 \psi\right) \rho^2. \tag{2.35}$$

We must in addition secure continuity of the tangential velocity component across the vortex boundary and vanishing of the normal velocity component at the vortex boundary. Equations (2.31) and (2.32) together ensure this, provided the function $R(\theta)$ is single valued, as we have tacitly assumed.

3. Numerical solution by finite differences

Here we describe a scheme for obtaining numerical solutions to (2.34) and (2.35) subject to the boundary conditions (2.29), (2.30) and (2.33) and the matching conditions on the vortex boundary (2.31) and (2.32). We use fourth-order-accurate finite differences in the domain $0 \leqslant \theta \leqslant \pi/2$, $0 \leqslant r < \infty$. A difficulty arises in treatment of the matching conditions on the unknown vortex boundary $r = R(\theta)$, because when $M_\infty > 0$, this boundary does not correspond to a coordinate line in r, θ independent variables. This was handled by use of the stretching coordinate transformation

$$\xi = \xi(r, \theta) = \frac{r}{r + R(\theta)}, \qquad \theta' = \theta. \tag{3.1}$$

This maps $r = R(\theta)$ into $\xi = \frac{1}{2}$, $0 \leqslant \theta' \leqslant \pi/2$ and $r \to \infty$ into $\xi = 1$, $0 \leqslant \theta' \leqslant \pi/2$. We henceforth omit the prime on the transformed theta variable. Additionally, we make the transformation of dependent variables, motivated by (2.29)

$$\psi = \Psi + \tfrac{1}{2} r^2 \sin^2 \theta. \tag{3.2}$$

These transformations give two nonlinear PDEs for $\Psi(\xi, \theta)$ and $\rho(\xi, \theta)$, $0 \leqslant \theta \leqslant \pi$, subject to the boundary conditions

$$\Psi = 0 \quad \text{on } \xi = 1, \tag{3.3}$$

$$\rho = 1 \quad \text{on } \xi = 1, \tag{3.4}$$

$$\Psi(\tfrac{1}{2}, \theta) = -\tfrac{1}{2} R^2(\theta) \sin^2\theta, \tag{3.5}$$

$$\left.\frac{\partial \Psi}{\partial \xi}\right|_{\xi=\frac{1}{2}} \quad \text{is continuous across } \xi = \tfrac{1}{2}, \tag{3.6}$$

and

$$\Psi = O(\xi^2) \quad \text{as } \xi \to 0. \tag{3.7}$$

These equations and the above boundary conditions contain dependence on $R(\theta)$, which must be determined as part of the solution. Symmetry about the the plane $\theta = \pi/2$ is assumed and is enforced by applying the boundary condition $\partial\Psi/\partial\theta|_{\theta=\pi/2} = 0$, $\xi \geqslant 0$. This is a statement that the vortex always has fore-aft symmetry. It means we need only consider the domain $\mathscr{D} \equiv [0 \leqslant \xi \leqslant 1;\ 0 \leqslant \theta \leqslant \pi/2]$.

Finite difference solutions to the mapped equations were sought on two regular grids in $\mathscr{D}$, $(\xi_i, \theta_j) = (i\,\Delta_1\xi, j\,\Delta\theta), i = 1, ..., I_1,\ j = 0, ..., J$, $(\xi_i, \theta_j) = (\tfrac{1}{2} + i\,\Delta_2\xi, j\,\Delta\theta), i = 0, ..., I_2, j = 0, ..., J$, where $\Delta_1\xi = 1/(2I_1)$, $\Delta_2\xi = 1/(2I_2)$ and $\Delta\theta = \pi/(2J)$. These grids join at the vortex boundary $\xi = \frac{1}{2}$. The vortex boundary $R(\theta)$ is represented by discrete points $R_j = R(j\Delta\theta)$, $j = 0, ..., J$. Finite-differenced forms of the governing PDEs were applied at interior points. These exclude the vortex axis $\theta = 0$, the origin $\xi = 0$, both of which are coordinate singularities, the vortex boundary $\xi = \frac{1}{2}$ and the outer boundary of $\mathscr{D}$ but do include the line of symmetry $\theta = \pi/2$. Five-point fourth-order-accurate stencils were used for all Ψ-derivatives. This gives $4J(I_1 + I_2 - 2)$ equations. Along the vortex boundary Ψ is fixed by (3.5), but its ξ-derivatives are unknown. By incorporating (3.5), a special form of (2.35) can be constructed on $\xi = \frac{1}{2}$ which when applied at $\theta = j\Delta\theta$, $j = 1, ..., J$, gives J equations. A further J equations result from satisfying (3.6) at these same points by equating $\partial\Psi/\partial\xi$ evaluated by five-point one-sided differences on each side of $\xi = \frac{1}{2}$. Equation (2.34) was not satisfied explicitly on the vortex boundary.

On the axis excluding both the origin and the stagnation point $\theta = 0, \xi = \frac{1}{2}$, a special form of the energy equation was satisfied. The stream function close to the axis must be of the form $\psi = \frac{1}{2} b(r) r^2 \theta^2 + \cdots$, where $b(r)/\rho(r)$ is the local axial velocity. Using (3.1), (3.2) and expressing $q(r)$ in term of Ψ-derivatives at $\theta = 0$ then gives a special form of (2.35) valid on $\theta = 0$ as

$$\frac{M_\infty^2}{2}\left(1 + \frac{(1-\xi)^2}{\xi^2 R^2(0)} \left.\frac{\partial^2\Psi}{\partial\theta^2}\right|_{\theta=0}\right)^2 + \frac{\rho^2}{\gamma - 1}\left(\rho^{\gamma-1} - 1\right) - \tfrac{1}{2} M_\infty^2 \rho^2 = 0. \tag{3.8}$$

Using centred finite differences for the Ψ-derivatives in (3.8) then gives $I_1 + I_2 - 2$ additional equations.

The coordinate singularity $r = 0$ is a well known source of difficulty for finite differences in polar coordinates. Several different strategies were employed with similar results. We give here a method based on applying a limiting form of the energy equation when $r \to 0$. Near the origin ψ must be take the form $\psi = \frac{1}{2} q_0 r^2 \sin^2\theta + \cdots = \frac{1}{2} q_0 R^2(\theta)\xi^2 \sin^2\theta + O(\xi^3)$. Letting $\xi \to 0$ in (2.35) and averaging over $0 \leqslant \theta \leqslant \pi/2$ then gives

$$\frac{M_\infty^2}{2}\left(1 + \frac{4}{\pi}\int_0^{\pi/2} \frac{1}{R^2(\theta)^2} \left.\frac{\partial^2\Psi}{\partial\xi^2}\right|_{\xi=0}\right)^2 + \frac{\rho_0^2}{\gamma - 1}\left(\rho_0^{\gamma-1} - 1\right) - \tfrac{1}{2} M_\infty^2 \rho_0^2 = 0, \tag{3.9}$$

where ρ_0 is the density at the origin. The Ψ-derivatives at $\xi = 0$ were evaluated

by one-sided differences based on a special stencil constructed using the form $\Psi = a_2(\theta)\,\xi^2 + a_3(\theta)\,\xi^3$ near $\xi = 0$, and the integral was calculated using a Newton–Cotes formula.

The above method can be shown to give a total of $(2J+1)\times(I_1+I_2-1)$ nonlinear equations for an equal number of unknowns which include the R_j, $j = 0, ..., J$. Thus M_∞ remains a free parameter and we have a one-parameter branch. This will be seen to be consistent with the Rayleigh–Janzen expansion to be described in the next section. The equations were solved by an approximate Newton method. Components of the Jacobian associated with$(\Psi - \rho)$ unknowns at grid points were evaluated analytically using a second-order–accurate finite-differenced version of (2.34)–(2.35) and (3.11)–(3.12). Derivatives with respect to the R_j unknowns were evaluated by second-order finite differences operating on the residuals. This scheme may be shown to give an 'arrowhead' Jacobian containing a banded structure, with bandwidth $8J+5$, together with two borders of width $J+1$. The resulting linear system was solved by a standard method using a code supplied by B. Fornberg. Owing to the approximation to the the true Jacobian, only linear convergence was obtained. With M_∞ fixed, this method was used to obtain numerical solutions to the nonlinear set of equations with averaged residuals not exceeding 10^{-9} in magnitude. The homentropic branch was investigated by continuing in M_∞ from the known analytic solution at $M_\infty = 0$.

4. The Rayleigh–Janzen expansion

We expand the solution in powers of M_∞^2, so that

$$\psi = \psi_0 + M_\infty^2\psi_1 + M_\infty^4\psi_2 + \cdots, \tag{4.1}$$

$$\rho = 1 + M_\infty^2\rho_1 + M_\infty^4\rho_2 + \cdots, \tag{4.2}$$

and

$$R(\theta) = 1 + M_\infty^2 R_1(\theta) + M_\infty^4 R_2(\theta) + \cdots. \tag{4.3}$$

On substituting into (2.34) and (2.35) we find that

$$\mathrm{D}^2\psi_0 = r^2\sin^2\theta\,\Omega_0, \tag{4.4a}$$

$$\mathrm{D}^2\psi_1 = N(\psi_0,\rho_1) + 2\rho_1\Omega_0 r^2\sin^2\theta, \tag{4.4b}$$

$$\mathrm{D}^2\psi_2 = -\rho_1 N(\psi_0,\rho_1) + N(\psi_0,\rho_2) + N(\psi_1,\rho_1) + (2\rho_2 + {\rho_1}^2)r^2\sin^2\theta\,\Omega_0, \tag{4.4c}$$

. . . . . .

and

$$\rho_1 = \tfrac{1}{2} + \Omega_0\psi_0 - \frac{1}{2r^2\sin^2\theta}\,N(\psi_0,\psi_0), \tag{4.5a}$$

$$\rho_2 = -\tfrac{1}{2}(\gamma+2){\rho_1}^2 + \rho_1 + \Omega_0(2\rho_1\psi_0 + \psi_1) - \frac{1}{r^2\sin^2\theta}\,N(\psi_0,\psi_1). \tag{4.5b}$$

. . . . . .

The operator D^2 takes the form

$$\mathrm{D}^2 = \frac{\partial^2}{\partial r^2} + \frac{(1-\mu^2)}{r^2}\frac{\partial^2}{\partial\mu^2}, \tag{4.6}$$

where $\mu = \cos\theta$.

Now ψ_0 is the stream function for the incompressible HSV and explicitly

$$\left.\begin{aligned} \psi_0 &= \tfrac{1}{2}\left(r^2 - 1/r\right)\left(1-\mu^2\right) \qquad (r>1), \\ \text{and} \qquad \psi_0 &= -\tfrac{3}{4} r^2\left(1-r^2\right)\left(1-\mu^2\right) \qquad (r<1). \end{aligned}\right\} \tag{4.7}$$

With ψ_0 to hand, we can calculate ρ_1 from (4.5*a*). Then the right-hand side of (4.4*b*) is determined and ψ_1 calculated. We next calculate ρ_2 from (4.5*b*) and then the right-hand side of (4.4*c*) is determined. Clearly, we can proceed in this way to compute the complete expansion.

This computation is helped by the observation that the right-hand side of each member of the system possesses a factor $1-\mu^2$. We can see this by noting that

$$N(f,g) = \frac{\partial f}{\partial r}\frac{\partial g}{\partial r} + \frac{\left(1-\mu^2\right)}{r^2}\frac{\partial f}{\partial \mu}\frac{\partial g}{\partial \mu}, \tag{4.8}$$

so that if f contains a factor $1-\mu^2$, so does $N(f,g)$. This suggests that we define $\overline{\psi}_n$ by

$$\psi_n = \left(1-\mu^2\right)\overline{\psi}_n. \tag{4.9}$$

This means that, provided $\overline{\psi}_n$ is a well-behaved function of μ, $\psi_n = 0$ on the axis of symmetry $\mu = 1$. Hence it must vanish on the vortex boundary as well, so that (2.31) is satisfied. We can take a further step by noting that ψ and ρ are even functions of μ and that this property is inherited by each right-hand side of the system (4.4). This suggests that we express the right-hand sides in the form

$$\left(1-\mu^2\right)\sum_s f_s(r) P'_{2s+1}(\mu). \tag{4.10}$$

Now

$$\mathrm{D}^2\left[\left(1-\mu^2\right)P'_{2s+1}(\mu) g_s(r)\right] = \left(1-\mu^2\right)P'_{2s+1}(\mu)\left(\frac{\mathrm{d}^2 g_s}{\mathrm{d}r^2} - \frac{g_s}{r^2}(2s+1)(2s+2)\right), \tag{4.11}$$

so that the problem of integrating the system (4.4) is reduced to solving equations of the form

$$\frac{\mathrm{d}^2 g_s}{\mathrm{d}r^2} - \frac{g_s}{r^2}(2s+1)(2s+2) = f_s(r). \tag{4.12}$$

This is facilitated by the change of variable $r = \mathrm{e}^t$, which yields

$$\frac{\mathrm{d}^2 g_s}{\mathrm{d}t^2} - \frac{\mathrm{d}g_s}{\mathrm{d}t} - (2s+1)(2s+2) g_s = \mathrm{e}^{2t} f_s(\mathrm{e}^t). \tag{4.13}$$

Detailed calculation, using Mathematica both to compute the right-hand sides (4.10) and to solve the equations (4.12), leads to solutions of the form

$$\psi_1 = \left(1-\mu^2\right)\left(f_0^{(1)}(r)\, P'_1(\mu) + f_1^{(1)}(r)\, P'_3(\mu)\right), \tag{4.14}$$

$$\psi_2 = \left(1-\mu^2\right)\left(f_0^{(2)}(r)\, P'_1(\mu) + f_1^{(2)}(r)\, P'_3(\mu) + f_2^{(2)}\, P'_5(\mu)\right); \tag{4.15}$$

we work to $O(M_\infty^4)$ from now on.

Each function $f_b^{(a)}$ contains the solution of the homogeneous equation

$$\frac{\mathrm{d}^2 g_s}{\mathrm{d}t^2} - \frac{\mathrm{d}g_s}{\mathrm{d}t} - (2s+1)(2s+2) g_s = 0, \tag{4.16}$$

namely

$$Ae^{-(2s+1)t} + Be^{(2s+2)t}.$$

If we are determining ψ outside the vortex, $B = 0$ by the conditions at infinity, while if we are determining ψ inside the vortex $A = 0$, by the requirement that ψ be well-behaved at the origin.

Hence, allowing for both exterior and interior forms of ψ, (4.14) and (4.15) show that we have 10 constants of integration to determine before the solution is complete. Our next task is to show how the boundary conditions (2.31) and (2.32) accomplish this.

We express the equation of the boundary in the form

$$R(\theta) = 1 + M_\infty^2 w_1(\theta) + M_\infty^4 w_2(\theta) + \cdots. \tag{4.17}$$

Then, for either the exterior or interior stream function, (2.31) insists that

$$\psi\left(1 + M_\infty^2 w_1 + M_\infty^4 w_2 + 0(M_\infty^6), \theta\right) = 0; \tag{4.18}$$

so applying Taylor's theorem,

$$\psi(1,\theta) + \left(M_\infty^2 w_1 + M_\infty^4 w_2 + 0(M_\infty^6)\right)\frac{\partial\psi}{\partial r}(1,\theta) + \tfrac{1}{2}\left(M_\infty^2 w_1 + \cdots\right)^2 \frac{\partial^2\psi}{\partial r^2} + \cdots = 0. \tag{4.19}$$

We now expand ψ as in (4.1) and on collecting the terms in 1, M_∞^2 and M_∞^4 and equating to zero we find

$$\psi_0(1,\theta) = 0, \tag{4.20a}$$

$$\psi_1(1,\theta) + w_1\frac{\partial\psi_0}{\partial r}(1,\theta) = 0, \tag{4.20b}$$

$$\psi_2(1,\theta) + w_2\frac{\partial\psi_0}{\partial r}(1,\theta) + w_1\frac{\partial\psi_1}{\partial r}(1,\theta) + \tfrac{1}{2}w_1^2\frac{\partial^2\psi_0}{\partial r^2}(1,\theta) = 0. \tag{4.20c}$$

Next, we must impose (2.32) which gives

$$\frac{\partial\psi^{(+)}}{\partial r}\left(1 + M_\infty^2 w_1 + M_\infty^4 w_2 + \cdots, \theta\right) = \frac{\partial\psi^{(-)}}{\partial r}\left(1 + M_\infty^2 w_1 + M_\infty^4 w_2 + \cdots, \theta\right), \tag{4.21}$$

where the suffix $(+)$ means outside the vortex and the suffix $(-)$ means inside the vortex. Expansion of ψ as in (4.1) and collection of terms leads to

$$\frac{\partial\psi_0^{(+)}}{\partial r} = \frac{\partial\psi_0^{(-)}}{\partial r}, \tag{4.22a}$$

$$\frac{\partial\psi_1^{(+)}}{\partial r} + w_1\frac{\partial^2\psi_0^{(+)}}{\partial r^2} = \frac{\partial\psi_1^{(-)}}{\partial r} + w_1\frac{\partial^2\psi_0^{(-)}}{\partial r^2}, \tag{4.22b}$$

$$\frac{\partial\psi_2^{(+)}}{\partial r} + w_1\frac{\partial^2\psi_1^{(+)}}{\partial r^2} + w_2\frac{\partial^2\psi_0^{(+)}}{\partial r^2} + \tfrac{1}{2}w_1^2\frac{\partial^3\psi_0^{(+)}}{\partial r^3} = \frac{\partial\psi_2^{(-)}}{\partial r} + w_1\frac{\partial^2\psi_1^{(-)}}{\partial r^2} + w_2\frac{\partial^2\psi_0^{(-)}}{\partial r^2} + \tfrac{1}{2}w_1^2\frac{\partial^3\psi_0^{(-)}}{\partial r^3}. \tag{4.22c}$$

We recall that ψ_s contains a factor $1 - \mu^2$ which can be cancelled throughout the systems (4.21) and (4.22). Equations (4.20*b*,*c*) show that w_1 is linear in μ^2 and w_2 is quadratic in μ^2 so, accordingly

$$w_1 = A_1 + A_2\mu^2, \tag{4.23}$$

and

$$w_2 = B_1 + B_2\mu^2 + B_3\mu^4. \tag{4.24}$$

Now the functions $\psi_1^{(+)}$, $\psi_1^{(-)}$, $\psi_2^{(+)}$ and $\psi_2^{(-)}$ contain ten constants, as we have seen. We have thus 15 constants to determine. Equation (4.20*b*) is linear in μ^2, so since it holds for both $\psi_1^{(+)}$ and $\psi_1^{(-)}$, it yields four equations. Equation (4.20*c*) is quadratic in μ^2 and thus yields six equations. The continuity conditions (4.22) similarly yield five equations, so that the boundary conditions (4.20) and (4.22) together yield 15 equations. Of course, this does not prove that the 15 unknown constants can be found, but actual calculation shows the system is non-singular. We give the results only for the constants determining the shape, which are

$$\left.\begin{aligned} A_1 &= \frac{155}{672}, \quad A_2 = \frac{17}{32}, \\ B_1 &= -\frac{7597469753}{61347686400} + \frac{842513627}{12415603200}\,\gamma, \\ B_2 &= -\frac{3436748983}{54628654080} + \frac{6536261}{31834880}\,\gamma, \quad B_3 = \frac{199522751}{472975360} - \frac{59607}{826880}\,\gamma. \end{aligned}\right\} \tag{4.25}$$

We can deduce that the axis ratio of the shape of the vortex is

$$R(0)/R(\pi/2) = 1 + 0.53125\,M_\infty^2 + (0.23640 + 0.13323\,\gamma)\,M_\infty^4 + O(M_\infty^6), \tag{4.26}$$

so that the effect of compressibility is to make the vortex prolate. The effect of compressibility on the speed of propagation can be measured by the dimensionless group

$$G \equiv U_\infty R(\pi/2)/|\Gamma|,$$

where Γ is the circulation around the vortex in any axial half-plane. Now

$$\Gamma = -\Omega_0 \int_0^\pi \int_0^{R(\theta)} \rho(r,\theta) r^2 \sin\theta \,\mathrm{d}r\,\mathrm{d}\theta, \tag{4.27}$$

so that

$$G \equiv U_\infty R(\pi/2)/|\Gamma| = 0.2 - 0.10565\,M_\infty^2 + (0.01568 - 0.026082\gamma)\,M_\infty^4 + O(M_\infty^6). \tag{4.28}$$

The results were checked by substituting $\psi(R,\theta)$ and $\rho(R,\theta)$ in the exact governing equations (2.34) and (2.35) and expanding the results of these substitutions in powers of M_∞^2, Mathematica being used to carry out the algebra. It was verified that the terms in 1, M_∞^2 and M_∞^4 vanished. The same procedure was used on the exact boundary conditions (2.31) and (2.32). As a further check the circulation Γ was calculated from

$$\int_{-\infty}^{\infty} (u-1)\mathrm{d}x, \tag{4.29}$$

where $u(x)$ is the velocity along the axis of symmetry, given by

$$u(x) = \frac{1}{\rho\, r^2\, \sin\theta} \left.\frac{\partial\psi}{\partial\theta}\right|_{\theta=0}; \tag{4.30}$$

because ψ contains a factor $\sin^2\theta$, the limit $\theta \to 0$ can be taken.

M_∞	Property	[20,16;32]	[40,32;64]	Ext.[0]	*R-J*, $O(M^4)$
0	$R(0)$	1.004 97	1.000 22	0.999 90	1.0
0	$R(\pi/2)$	1.004 97	1.000 22	0.999 90	1.0
0	G	0.198 02	0.199 82	0.199 94	0.2
0.1	$R(0)$	1.013 39	1.008 20	1.007 85	1.007 67
0.1	$R(\pi/2)$	1.007 66	1.002 80	1.002 47	1.002 30
0.1	ρ_0	0.993 45	0.993 68	0.993 70	0.993 72
0.1	M_0	0.151 64	0.150 57	0.150 50	0.150 46
0.1	G	0.196 79	0.198 74	0.198 87	0.198 94
0.3	$R(0)$	1.086 75	1.074 37	1.073 55	1.072 76
0.3	$R(\pi/2)$	1.029 76	1.021 45	1.020 89	1.020 53
0.3	ρ_0	0.938 02	0.941 24	0.941 45	0.941 44
0.3	M_0	0.468 82	0.462 91	0.462 52	0.462 16
0.3	G	0.186 64	0.189 94	0.190 16	0.190 32
0.5	$R(0)$	1.279 97	1.230 74	1.227 46	1.222 76
0.5	$R(\pi/2)$	1.078 35	1.055 84	1.054 34	1.055 86
0.5	ρ_0	0.812 97	0.833 68	0.835 06	0.825 96
0.5	M_0	0.831 82	0.803 89	0.802 03	0.805 16
0.5	G	0.163 72	0.171 37	0.171 88	0.172 28

TABLE 1. Principal solution parameters for $M_\infty = 0$, 0.1, 0.3, 0.5 using each of two grids, $[I_1, I_2; J] = [20, 16; 32]$ and $[I_1, I_2; J] = [40, 32; 64]$. $G = U_\infty R(\pi/2)/|\Gamma|$. Also shown are values obtained from Richardson extrapolation assuming fourth-order accuracy and results from the Rayleigh–Janzen expansion to $O(M_\infty^4)$.

5. Results and discussion

We discuss solutions to the finite-difference formulation described in §3 obtained using two grids, $[I_1, I_2; J] = [20, 16; 32]$ and $[I_1, I_2; J] = [40, 32; 64]$. These were found by starting with the known solution for $M_\infty = 0$ and incrementing M_∞ along the homentropic branch. For all solutions we use $\gamma = 1.4$ unless otherwise specified. Table 1 lists some principal solution parameters obtained from the numerical solutions at several values of M_∞ compared with the predictions of the Rayleigh–Janzen expansion. Numerical values obtained using the two grids are shown in the third and fourth column respectively. The fifth column displays values obtained by the use of Richardson extrapolation with the assumption of fourth-order accuracy. There is generally near four-figure agreement with the Rayleigh–Janzen results, although we note that the discrepancy is somewhat larger than one might expect at our smallest finite value $M_\infty = 0.1$, where errors in the Rayleigh–Janzen calculation are expected to be uniformly of $O(10^{-6})$. This may be attributable to some loss of accuracy at the coordinate singularity $r = 0$ produced by our strategy of averaging over θ. It is well known that this can degrade global accuracy. We were unable to perform calculation with $[I_1, I_2; J] = [80, 64; 128]$ which would be required to confirm our estimate of fourth-order accuracy of the finite difference method.

In figures 1–3 we show contours of $\psi(x, y)$, $\rho(x, y)$, and $M(x, y)$ respectively for $M = 0.5$ in an axial plane with $x = r\cos\theta$ and $y = r\sin\theta$. The slight prolate shape of the vortical bubble with aspect ratio $R(0)/R(\pi/2) = 1.040$ is evident. The density contours show the density first increasing along the axis as we move towards the vortex from infinity, becoming maximum at the stagnation point where the bubble boundary intersects the axis, then decreasing to a value $\rho_0 = 0.834$ at the origin, or vortex geometrical centre. The Mach number contours of figure 3 show two regions where

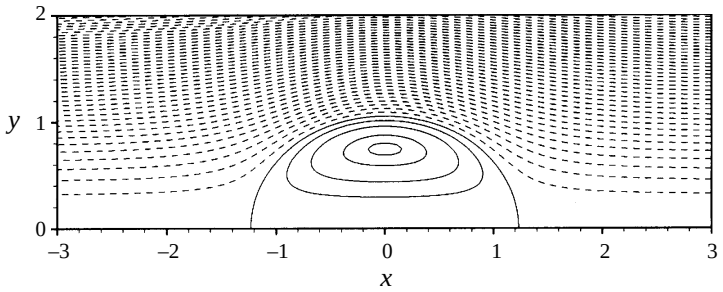

FIGURE 1. Contours of stream function ψ for a compressible Hill's spherical vortex $M_\infty = 0.5$. Solid lines $\psi < 0$. Dotted lines $\psi > 0$. Coordinates $x = r\cos\theta$, $y = r\sin\theta$.

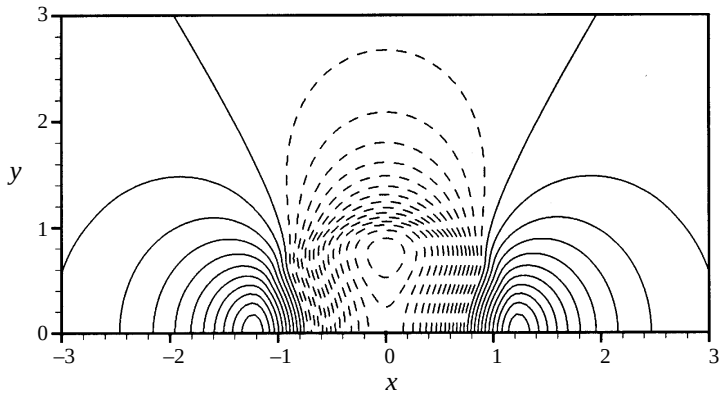

FIGURE 2. Contours of density ρ for a compressible Hill's spherical vortex $M_\infty = 0.5$. Solid lines $\rho > 1$. Dotted lines $\rho < 1$.

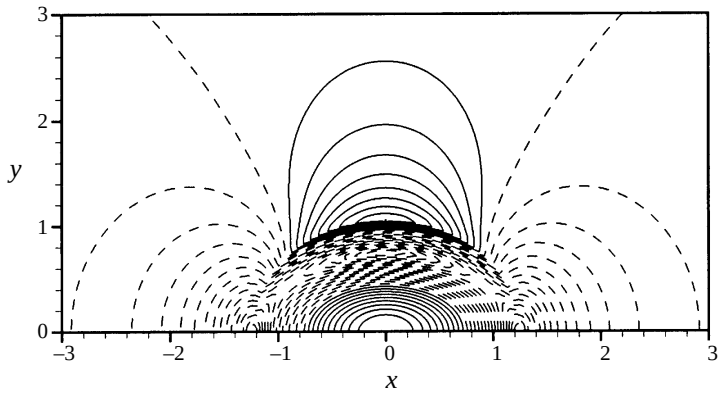

FIGURE 3. Contours of local Mach number for a compressible Hill's spherical vortex $M_\infty = 0.5$. Solid lines $M > M_\infty$. Dotted lines $M < M_\infty$.

$M(x, y) > M_\infty$, one surrounding the vortex centre where the contours of constant M are elliptical, and another in the irrotational stream just outside the vortex boundary. As M_∞ is increased along the homentropic branch the aspect ratio of the vortex increases slightly as may be seen from the entries in table 1, the detailed vortex boundary shapes of figure 4 and the plot of $R(0)$ and $R(\pi/2)$ versus M_∞ in figure 5.

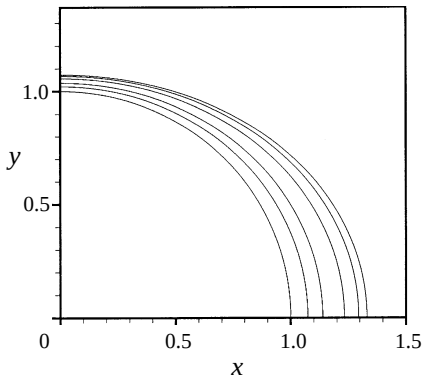

FIGURE 4. Shape of vorticity boundary. From inside moving outwards, $M_\infty = 0.3, 0.4, 0.5, 0.55, 0.575$.

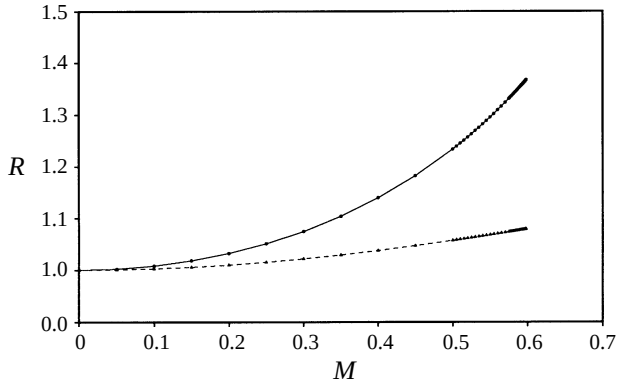

FIGURE 5. $R(0)$ (dashed line) and $R(\pi/2)$ (solid line) versus M_∞. Symbols show computed values.

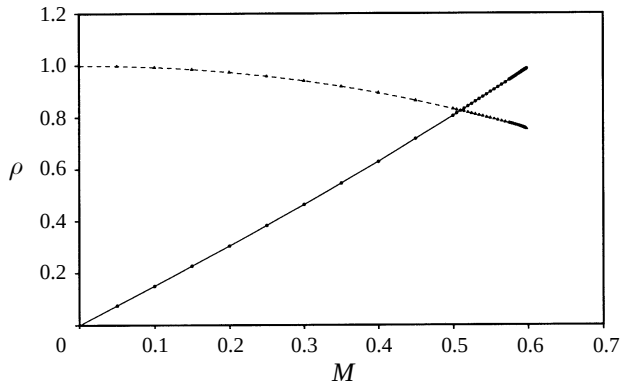

FIGURE 6. Density ρ_0 (dashed line) and Mach number M_0 (solid line) at origin $x = y = 0$.

The finite-difference computations were continued to a value $M_\infty = 0.598$ near which, with our maximum resolution $[I_1, I_2; J] = [40, 32; 64]$, the Jacobian became nearly singular. No converged solutions with $M_\infty > 0.598$ could be found. Figure 6 shows the gas density ρ_0 and Mach number M_0 at the the origin of coordinates, or vortex geometrical centre $r = 0$, versus M_∞. At $M_\infty = 0.598$ we find $\rho_0 = 0.7543$,

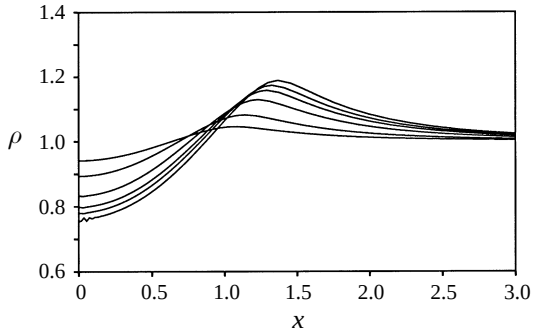

FIGURE 7. Density ρ along vortex axis. In order of decreasing density at $x = 0$, $M_\infty = 0.3, 0.4, 0.5, 0.55, 0.575, 0.598$.

from which M_0 can be obtained from

$$M_0^2 = \frac{1}{\rho_0^{\gamma-1}} \left[M_\infty^2 - \frac{2}{\gamma - 1} \left(\rho_0^{\gamma-1} - 1 \right) \right], \tag{5.1}$$

giving $M_0 = 0.9986$. The flow is thus nearly sonic at $r = 0$ for our largest M_∞ and a detailed examination of the $M(r, \theta)$ field for this case showed that the flow was nowhere locally supersonic. Thus we do not find numerical solutions for the compressible Hill's spherical vortex corresponding to transonic flow. The value of M_∞ for which $M_0 = 1$ can be estimated from the Rayleigh–Janzen expansion by using the perturbation solution to evaluate the density ρ_0 and the velocity q_0 at $r = 0$, with the result that

$$\rho_0 = 1 - \tfrac{5}{8} M_\infty^2 - \left(\frac{5}{448} + \frac{25\gamma}{128} \right) M_\infty^4, \tag{5.2}$$

$$q_0 = \tfrac{3}{2} + \tfrac{15}{56} M_\infty^2 - \left(\frac{3386709}{9865856} - \frac{639\gamma}{9152} \right) M_\infty^4. \tag{5.3}$$

A straightforward calculation shows that $M_0 = M_\infty q_0 / \rho_0^{(\gamma-1)/2}$. Substituting (5.2) and (5.3) into this expression and expanding $q_0/\rho_0^{(\gamma-1)/2}$ to $O(M_\infty^4)$ then gives an estimate of M_0 from the Rayleigh–Janzen expansion. On putting $M_0 = 1$, $\gamma = 1.4$ and solving for M_∞ we find $M_\infty = 0.60308$ in fair agreement with the finite-difference result. Profiles of the gas density $\rho(x)$ and local Mach number $M(x)$ along the vortex axis $r = x$ are shown in figures 7 and 8 respectively for several values of M_∞ in the range $0.3 \leqslant M_\infty \leqslant 0.598$. Near $x = 0$ there may be seen some non-smoothness in the profiles which appears to be associated with the coordinate singularity. This was found to increase when $M_\infty \to 0.598$ as can be clearly seen in these plots.

There are several possible reasons for our failure to find transonic flow solutions. One is that there is a turning point at or near $M_\infty = 0.598$. Several attempts were made to continue in other parameters such as $R(0)$, $R(\pi/2)$, or ρ_0, and in addition the code was modified to allow arclength continuation in the space of all of the parameters of the discrete problem. These were not successful, the branch from M_∞ terminating in each case very near $M_\infty = 0.598$. A second possibility is that the branch terminates where the flow becomes locally supersonic owing to the development of a singularity. A third possibility is that solutions with locally supersonic flow require the breaking of fore-aft symmetry of the vortex structure imposed by us in the problem

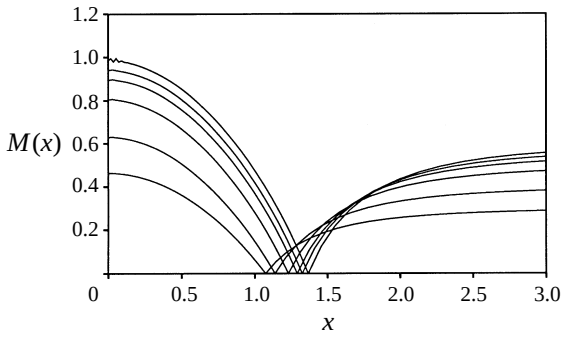

FIGURE 8. Mach number $M(x)$ along vortex axis. In order of increasing Mach number at $x = 0$, $M_\infty = 0.3$, 0.4, 0.5, 0.55, 0.575, 0.598.

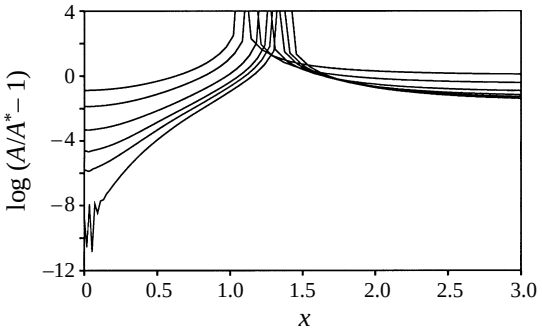

FIGURE 9. Area ratio $A(x)/A^*$ plotted as $\log(A(x)/A^* - 1)$ along vortex axis.

formulation. The flow along the axis can be viewed as one-dimensional flow with area change, from which it is well known that along a one-dimensional streamtube, the flow can be either symmetrical about a point of minimum streamtube area with subsonic velocities on both sides, or else subsonic on one side and supersonic on the other side of an asymmetrical streamtube. With the present imposed symmetries, the only way the latter can can occur is if a double throat is formed along the axial streamtube, with one area minimum in each half of the vortex. Figure 9 shows a plot of $\log[A(x)/A^* - 1]$ where $A(x)/A^*$ is the one-dimensional area ratio given by

$$\frac{A(x)}{A^*} = \frac{1}{M(x)}\left[\frac{2}{\gamma - 1}\left(1 + \frac{\gamma - 1}{2} M(x)^2\right)\right]^{\frac{\gamma+1}{2(\gamma-1)}}, \tag{5.4}$$

where A^* is the sonic area and $M(x)$ is the axial Mach number distribution of figure 8. Figure 9 shows that $A(x)/A^* - 1$ is very slowly varying near $x = 0$, so that the axial streamtube is very nearly of constant area along much of the axis within the vortex. This was confirmed by a detailed study of the near-axial contours of ψ. We find no evidence of the formation of a double throat streamtube geometry although we cannot rule this out. Of course if locally supersonic solutions do exist, it may be that the flow first becomes supersonic just off the axis, as is known to occur for Laval nozzle flow, (e.g. see Shapiro 1954, p. 828), and that the double nozzle streamline geometry, with axial supersonic flow appears only at larger Mach number. A fourth scenario is that our treatment of the coordinate singularity is not sufficiently refined to capture the transition to supersonic flow. This cannot be ruled out.

Lastly we mention an attempt to investigate a possible broken branch, in which the existence of symmetrical shockless transonic solutions resume at $M_\infty > 0.598$, following a gap along the real M_∞ line. To do this, we turned on complex arithmetic, thus complexifying our code and allowing solutions in a space of complex Mach number $M_\infty = M_\infty^R + \mathrm{i}\, M_\infty^I$ where M_∞^R and M_∞^I are the real and complex part respectively. In this complexification, the physical parameters defining the solution such as involve the boundary conditions and the various step sizes are of course kept real. We found no difficulty in obtaining complex-valued solutions along trajectories in the $M_\infty^R + \mathrm{i}\, M_\infty^I$ plane along which $M_\infty^R > 0.598$, $|M_\infty^I| \neq 0$. However all attempts to return to the real axis for $M_\infty^R > 0.598$ were unsuccessful. In fact it was always found that as the real M_∞ axis was approached from above and below with $M_\infty^R > 0.598$, the respective solutions appeared to approach complex conjugate states. This suggests the presence of a branch cut extending along the real axis from $M_\infty^R = 0.598$. We note the presence of an obvious source of non-analyticity in our basic equations (2.34) and (2.35) through the fractional powers of ρ. However even with integral γ, non-analyticity remains. Consider for example $\gamma = 2$. Equation (2.35) can then in principle be solved for ρ as a function of the ψ-derivatives, and substitution into (2.39) then gives a single equation for ψ. Non-analyticity remains however because (2.35) is a cubic equation for ρ. In fact calculation with $\gamma = 2$ produced very similar qualitative behaviour to that described above for $\gamma = 1.4$.

6. Concluding remarks

We have constructed both numerical and perturbation solutions which describe the steady propagation of an prolate-spheroidal-like vortex in a compressible ideal gas. These vortex states correspond to a homentropic continuation of the classical Hill's spherical vortex in an incompressible fluid, to finite Mach number. This continuation is not unique and we discuss in the Appendix two different admissible continuations, each corresponding to homenthalpic flow, in which $S = 0$ outside the vortex and $S = S(\psi)$ inside the vortex bubble. Of these, the first corresponds to a flow in which S is proportional to ψ within the vortex. We present no analysis or detailed solutions for this case. The second homenthalpic branch is shown to be generated from the present homentropic one by a transformation of the steady Euler equations due to Munk & Prim (1947). This gives an homenthalpic flow with the same vortex shape, general streamline pattern and Mach number distribution as the equivalent homentropic case at the same free-stream Mach number, but with different kinematic and thermodynamic properties internal to the vortex. These properties are determined by the Munk–Prim transformation.

The numerical evidence indicates that our homentropic branch is continuous from $M_\infty = 0$ to $M_\infty \approx 0.598$ at which value it terminates, probably due to non-analyticity near the vortex centre associated with the onset of locally transonic flow. An attempt to find a continuous branch of solutions or even isolated solutions for special values of $M_\infty > 0.598$ failed. Our evidence for the existence of a singularity terminating the homentropic branch rests mainly on the non-existence of a turning point, which itself indicates non-analyticity, and the behaviour of solutions to our complexified codes, which seem to indicate branch-point type behaviour. The axial streamtubes at Mach numbers close to $M_\infty = 0.598$ show extremely slow axial area variation near the incipient sonic point and this may indicate a very weak singularity.

The non-existence of a continuous family of shock-free transonic flow about airfoils of fixed shape is well known (Morawetz 1956, 1957, 1958). Barsony-Nagy, Er-El &

Youngster (1987), Moore & Pullin (1987) and Ardalan *et al.* (1995) have provided numerical and analytical evidence supporting the existence of continuous families of shock-free transonic flows with closed free-streamlines. In these flows an annulus of transonic irrotational flow surrounds the free streamlines, which can be viewed as embedded vortices. In view of this we are surprised at our failure to find compressible Hill's spherical vortices containing regions of smooth transonic flow. Our flow is different to those cited above in that nearly-sonic conditions first appear within the vortex, very near to and possibly right at the vortex geometrical centre. We know of no existence theorems relevant to transonic rotational flow with compact vorticity. The question of existence of this type of vortex-flow for non-trivial boundary conditions remains an open question.

D.I.P. was partly supported by a grant from the EPSERC of the UK. We acknowledge a referee who pointed out the relevance of the Munk–Prim transformation.

Appendix. Homenthalpic continuation

We demonstrate alternative continuations to $M_\infty > 0$ by considering homenthalpic flow. We start from (2.16) with the assumption that $H_0(\psi) = H_{00} = \text{const}$ throughout the fluid, with the result that

$$\frac{\eta}{r\,\sin\theta\rho\,T} = \frac{\mathrm{d}S}{\mathrm{d}\psi} \equiv W(\psi). \tag{A 1}$$

The entropy equation of state is

$$p = p_\infty\,\rho^\gamma \exp(S), \tag{A 2}$$

where p_∞ is the (dimensionless) pressure at infinity and where S has been made dimensionless against C_v, the specific heat at constant volume.

We make the function W dimensionless against the quantity $p_\infty a^2/R\,U_\infty$, where R is the gas constant. The dimensionless form of the right-hand side of (A 1) is then

$$\frac{\mathrm{d}S}{\mathrm{d}\psi} = \gamma\,(\gamma-1)\,M_\infty^2\,W(\psi). \tag{A 3}$$

In lieu of (2.24) we now choose $W(\psi) = -\Omega_0$:

$$\left.\begin{aligned} \Omega_0 &= \tfrac{15}{2} \qquad \text{(inside the HSV)},\\ \Omega_0 &= 0 \qquad\quad \text{(outside the HSV)}, \end{aligned}\right\} \tag{A 4}$$

and retain this value of $W(\psi)$ for the compressible case thus defining a homenthalpic continuation of the HSV to $M_\infty > 0$. Equation (A 3) can now be integrated to give

$$S = -\gamma\,(\gamma-1)\,M_\infty^2\,\Omega_0\,\psi. \tag{A 5}$$

Following the steps giving (2.34)–(2.35), while using (A 2), (A 4) and (A 5) and the equation of state for a perfect gas then gives the dimensionless forms of the vorticity and energy equations

$$\frac{\partial^2\psi}{\partial r^2} + \frac{1}{r^2}\left(\frac{\partial^2\psi}{\partial\theta^2} - \cot\theta\frac{\partial\psi}{\partial\theta}\right) - \frac{1}{\rho}\left(\frac{\partial\psi}{\partial r}\frac{\partial\rho}{\partial r} + \frac{1}{r^2}\frac{\partial\psi}{\partial\theta}\frac{\partial\rho}{\partial\theta}\right)$$
$$= \Omega_0\,\rho^{\gamma+1}\,r^2\sin^2\theta\exp\left(-\gamma\,(\gamma-1)M_\infty^2\Omega_0\psi\right), \tag{A 6}$$

and

$$\frac{M_\infty^2}{2r^2\sin^2\theta}\left[\left(\frac{\partial\psi}{\partial r}\right)^2+\frac{1}{r^2}\left(\frac{\partial\psi}{\partial\theta}\right)^2\right]$$

$$+\frac{\rho^2}{\gamma-1}\left[\rho^{\gamma-1}\exp\left(-\gamma(\gamma-1)M_\infty^2\Omega_0\psi\right)-1\right]=\tfrac{1}{2}M_\infty^2\rho^2. \tag{A 7}$$

Equations (A 6)–(A 7) define a homenthalpic continuation of the Hill's spherical vortex to compressible flow. The boundary conditions (2.29)–(2.33) remain unchanged. We have not solved (A 6)–(A 7) but presume that for fixed M_∞, they give a different detailed vortex structure to the homentropic case (2.34)–(2.35).

It may be shown that the above homenthalpic continuation of the incompressible HSV is not itself unique. We consider the transformation of Munk & Prim (1947) who showed that for every solution $[\boldsymbol{u}, p, \rho, T, H_0, S]$ of the steady Euler equations, there exists a set of further solutions $[\boldsymbol{u}^*, p^*, \rho^*, T^*, H_0^*, S^*]$ such that

$$\left.\begin{aligned}&\boldsymbol{u}^*=\lambda\,\boldsymbol{u},\quad \rho^*=\frac{1}{\lambda^2}\,\rho,\quad p^*=p,\\&T^*=\lambda\,T,\quad H_0^*=\lambda^2\,H_0,\quad S^*=S+\gamma\log\lambda^2,\end{aligned}\right\} \tag{A 8}$$

where $\lambda=\lambda(\psi)$ is an arbitrary function of ψ and $\mathrm{d}\psi^*/\mathrm{d}\psi=1/\lambda$. For swirl-free flow in our present spherical polar coordinates, the vorticities are related by

$$\eta^*=\lambda\,\eta-\rho\,r\,\sin\theta\,\boldsymbol{u}^2\left(\frac{\mathrm{d}\lambda}{\mathrm{d}\psi}\right). \tag{A 9}$$

It is straightforward to show that (2.16) is invariant under (A 8)–(A 9), as is local Mach number $M\equiv q/c=M^*=q^*/c^*$.

We now use this transformation applied to our homentropic flow to generate an equivalent homenthalpic flow, and show that this does not correspond to the continuation defined by (A 1)–(A 7). For our homentropic flow $S=0$, $H_0=H_{00}$ outside the vortex and $S=0$, $H_0=\Omega_0\psi+H_{00}$ inside, where $H_{00}=1/2+1/((\gamma-1)M_\infty^2)$. The equivalent homenthalpic flow has $H_0^*=H_{00}$ everywhere. It follows from (A 8) that ouside the vortex $\lambda=1$, $\eta^*=\eta=0$, $S^*=S=0$. Inside the vortex $H_0^*=H_{00}=\lambda^2\,H_0$, from which it follows, using $\lambda=d\psi/d\psi^*$, that

$$\frac{\mathrm{d}\psi^*}{\mathrm{d}\psi}=\frac{1}{H_{00}^{1/2}}\,(H_{00}+\Omega_0\,\psi)^{1/2}. \tag{A 10}$$

Integrating, using $\psi^*=0$ when $\psi=0$, and inverting the result gives

$$\psi=\frac{H_{00}^{1/3}}{2^{2/3}\,\Omega_0}\left(3\Omega_0\psi^*+2\,H_{00}\right)^{2/3}-\frac{H_{00}}{\Omega_0},\quad \lambda=\frac{2^{1/3}\,H_{00}^{1/3}}{(3\Omega_0\psi^*+2\,H_{00})^{1/3}}, \tag{A 11}$$

and we note that $\lambda=1$ when $\psi=0$. The entropy $S^*(\psi^*)$ follows from (A 8) and (A 12), from which can be obtained, for the equivqlent homenthalpic vortex, within the vortex itself

$$W^*(\psi^*)\equiv\frac{\mathrm{d}S^*}{\mathrm{d}\psi^*}=-\frac{2\Omega_0\gamma}{3\Omega_0\psi^*+2H_{00}}. \tag{A 12}$$

The streamline geometry, including the vortex-boundary shape, and the internal Mach number distribution for the equivalent homenthalpic vortex are identical to those for

the original homentropic vortex but the detailed internal distributions for the other flow properties differ for the two solutions.

Comparing (A 13) to (A 5) shows that these homenthalpic continuations of the Hill's spherical vortex to compressible flow are not equivalent. Moreover they apparently cannot be transformed into each other by a Munk–Prim transformation. Expansion of (A 13) in powers of M_∞^2, however, gives

$$\frac{\mathrm{d}S^*}{\mathrm{d}\psi^*} = -\gamma\,(\gamma-1)M_\infty^2\Omega_0 + \tfrac{1}{2}\,\gamma\,(\gamma-1)^2\,M_\infty^4\left(1+3\Omega_0\psi^*\right) + O(M_\infty^6). \tag{A 13}$$

Hence (A 5) and (A 14) agree to $O(M_\infty^2)$, when M_∞^2 is small.

REFERENCES

Ardalan, K., Meiron, D. I. & Pullin, D. I. 1995 Steady compressible vortex flows: the hollow-core vortex array. *J. Fluid Mech.* **301**, 1–17.

Barsony-Nagy, A., Er-El, J. & Youngster, S. 1987 Compressible flow past a contour and stationary vortices. *J. Fluid Mech.* **178**, 367–378.

Brown, S. N. 1965 The compressible viscous leading-edge vortex. *J. Fluid Mech.* **22**, 17–32.

Colonius, T., Lele, S. K. & Moin, P. 1991 The free compressible viscous vortex. *J. Fluid Mech.* **230**, 45–73.

Heister, S. D., McDonough, J. M., Karagozian, A. R. & Jenkins, D. W. 1990 The compressible vortex pair. *J. Fluid Mech.* **220**, 339–354.

Hill, M. H. M. 1894 On a spherical vortex. *Phil. Trans. R. Soc. Lond.* A **185**, 213–245.

Lee, S. & Bershader, D. 1994 The structure of compressible starting vortices. *Exps. Fluids* **16**, 248–254.

Lixian, Z., Sato, J. & Shimizu, S. 1997 A numerical study of the interaction between a moving shock wave and a spherical vortex. *Trans. Japan. Aero. Space Soc.* **40**, 49–57.

Mack, L. M. 1960 The compressible viscous heat conducting vortex. *J. Fluid Mech.* **8**, 284–292.

Moore, D. W. & Pullin, D. I. 1987 The compressible vortex pair. *J. Fluid Mech.* **185**, 171–204.

Morawetz, C. S. 1956 On the non-existence of continuous transonic flows past airfoils. I. *Commun. Pure Appl. Maths* **9**, 45–68.

Morawetz, C. S. 1957 On the non-existence of continuous transonic flows past airfoils. II. *Commun. Pure Appl. Maths* **10**, 107–131.

Morawetz, C. S. 1958 On the non-existence of continuous transonic flows past airfoils. III. *Commun. Pure Appl. Maths* **11**, 129–144.

Munk, M. & Prim, R. 1947 On the multiplicity of steady gas flows having the same streamline pattern. *Proc. Nat. Acad. Sci.* **33**, 137–141.

Samtaney, R. & Pullin, D. I. 1997 Shock interactions with a compressible Hill's spherical vortex. In *Proc. 21st Intl Symp. on Shock Waves. Paper 4710*, 6 pp.

Shapiro. A. H. 1954 *The Dynamics and Thermodynamics of Compressible Flow*, Vol. II. The Ronald Press, New York.

Vazsonyi, A. 1945 On rotational gas flows. *Q. J. Appl. Maths* **3**, 29–38.